Yas *et. al.,* Babcock Univ. Med. J.2026 9(S1):307-315
https://doi.org/10.38029/babcockuniv.med.j..v9iS1.1649
eISSN: 2756-4657

RESEARCH ARTICLE OPEN ACCESS

Antibacterial and antibiofilm synergy of silver selenium core-shell nanoparticles with meropenem against multidrug-resistant Klebsiella pneumoniae isolated from catheter-related urinary tract infections

Yas EF[1], Jameel SK[1], Mohammed MS[1]

[1]*Department of Microbiology, College of Medicine, Al-Iraqia University, Baghdad, Iraq*

Submitted: 8th May 2026
Accepted: 12th June 2026
Published: 31st October 2026
ID: Orcid ID

Abstract
Objective: To evaluate the antibacterial and antibiofilm efficacy of cold plasma-synthesised silver-selenium (Ag@Se) core–shell nanoparticles, alone and in combination with meropenem, against multidrug-resistant *Klebsiella pneumoniae* isolates from catheter-associated urinary tract infections.
Methods: Ag@Se nanoparticles were synthesised using an atmospheric cold plasma jet system. Characterisation was performed by UV-Vis spectroscopy, X-ray diffraction (XRD) and transmission electron microscopy (TEM). Cytotoxicity was assessed on rat embryo fibroblast (REF) cells. Among 200 urine samples, 67 *K. pneumoniae* isolates were identified; 30 were multidrug-resistant, and five highly resistant isolates with strong biofilm formation were selected for synergy testing using checkerboard assays. Biofilm formation was quantified by crystal violet microtiter plate method.
Results: XRD confirmed a face-centred cubic silver core; TEM showed core–shell structures of ~100 nm. Ag@Se nanoparticles exhibited low cytotoxicity (maximum growth inhibition 23.3 % at 48 h, 100 µg/mL). Against the five selected isolates, Ag@Se alone achieved 50–65 % growth inhibition. Combination with meropenem increased inhibition to 60–70 %. Synergy was confirmed by isobologram and combination index analyses.
Conclusion: Plasma-synthesised Ag@Se nanoparticles enhance meropenem activity against MDR *K. pneumoniae* and show acceptable biocompatibility, offering a promising nano-antibiotic strategy for biofilm-associated urinary tract infections.

Keywords: *Klebsiella pneumoniae,* silver-selenium nanoparticles, cold plasma, meropenem, biofilm, urinary tract infection

Plain English Summary

Urinary tract infections caused by *Klebsiella pneumoniae* are increasingly difficult to treat because the bacteria form protective biofilms and resist many antibiotics. In this study, scientists used a cold plasma device to create tiny particles made of silver and selenium (called Ag@Se nanoparticles). These particles were tested together with the antibiotic meropenem against bacteria from patients with catheter-related infections. The combination stopped up to 70 % of bacterial growth and was relatively safe for normal cells. This approach could lead to new treatments for stubborn urinary tract infections.

Introduction

Urinary tract infections (UTIs) remain a major clinical challenge worldwide, particularly in hospitalised patients and those with indwelling urinary catheters (1). *Klebsiella pneumoniae*, a Gram-negative encapsulated bacterium, is a

Correspondence:
Mohammed MS
Department of Microbiology, College of Medicine
Al-Iraqia University, Baghdad
Iraq
+9647700299632, mohammed.subhi@aliraqia.edu.iq

© BUMJ. 2026 Open Access This article is distributed under the terms of the Creative Commons Attribution 4.0 International License (http://creativecommons.org/licenses/by/4.0/), which permits unrestricted use, distribution, and reproduction in any medium, provided you give appropriate credit to the original author(s) and the source, provide a link to the Creative Commons license, and indicate if changes were made. The Creative Commons Public Domain Dedication waiver (http://creativecommons.org/publicdomain/zero/1.0/) applies to the data made available in this article, unless otherwise stated.

leading cause of catheter-associated UTIs. Its ability to form robust biofilms on catheter surfaces and to acquire multidrug resistance (MDR) has rendered many first-line antibiotics ineffective (2, 3). The emergence of extended-spectrum β-lactamases (ESBLs) and carbapenemases further complicates treatment, limiting therapeutic options to a handful of often toxic or costly agents (4).

Biofilms not only protect bacteria from host immune responses but also reduce antibiotic penetration, leading to persistent and relapsing infections (5). Hypervirulent strains with hypermucoviscous capsules (notably serotypes K1 and K2) exacerbate the problem by resisting phagocytosis and complement-mediated killing (6). In response to this crisis, nanomedicine has emerged as a promising frontier. Metal nanoparticles, particularly silver (Ag) and selenium (Se), exhibit multi-mechanistic antibacterial actions, including disruption of bacterial membranes, generation of reactive oxygen species (ROS), and interference with metabolic pathways (7, 8).

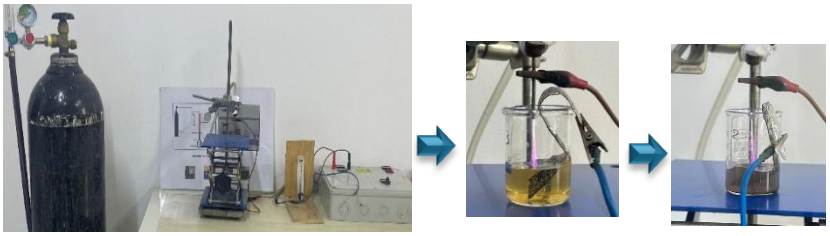
Green synthesis methods, such as cold atmospheric plasma (CAP), offer advantages over chemical reduction by eliminating toxic stabilisers and enabling precise control over particle size and morphology (9). Previous studies have shown that plasma-synthesised nanoparticles can be engineered with core–shell architectures to combine the properties of different metals (10). However, the synergistic potential of Ag@Se core–shell nanoparticles combined with meropenem against biofilm-forming, MDR *K. pneumoniae* has not been fully explored. Therefore, this study aimed to synthesise Ag@Se nanoparticles using a CAP system, characterise their physicochemical properties, assess their cytotoxicity, and evaluate their individual and synergistic antibacterial and antibiofilm activities against clinical isolates of *K. pneumoniae* from catheter-related UTIs.

Materials and Methods

Plasma jet system and nanoparticle synthesis

A cold atmospheric plasma jet system was constructed using a stainless steel capillary electrode (inner diameter 1 mm, length ~1 cm) powered by a DC high-voltage supply (10–20 kV, 25 kHz). Argon gas was flowed at 2.5 L/min through the capillary. The counter-electrode was a liquid precursor solution in a glass beaker placed 1 mm below the nozzle. This system reduced metal ions without chemical stabilisers.

Silver nanoparticles (AgNPs) were synthesised by exposing 1 mM silver nitrate ($AgNO_3$) in deionised water to the plasma for 4 minutes, producing a colour change from colourless to yellow. Selenium nanoparticles (SeNPs) were prepared from 0.5 mM selenium nitrate ($Se(NO_3)_3$) in deionised water with plasma exposure for 10 minutes. For Ag@Se core–shell nanoparticles, 5 mL of preformed AgNP colloid was mixed with 5 mL of 0.5 mM selenium nitrate solution and subjected to plasma for another 10 minutes, allowing selenium to deposit onto the silver cores.



(A) (B) (c)

Figure (1): synthesis of Ag@Se NPs (A) plasma jet system (B) Ag NPs as a core (C) Ag@Se NPs

Characterisation of nanoparticles

UV-Vis absorption spectra were recorded (200–800 nm) to detect surface plasmon resonance (SPR) peaks. X-ray diffraction (XRD) patterns were obtained using Cu-Kα radiation (λ=1.5406 Å) to identify crystalline phases. Transmission electron microscopy (TEM) was used to visualise particle size, morphology, and core–shell structure.

Cytotoxicity assay

Rat embryo fibroblast (REF) cells were cultured in RPMI 1640 medium with 10 % fetal bovine serum, 100 U/mL penicillin, and 100 µg/mL streptomycin at 37 °C in 5 % CO_2. Cells (10,000 per well) were seeded in 96-well plates and exposed to Ag@Se nanoparticles at 12.5, 25, 50, and 100 µg/mL for 24 and 48 hours. Viability was assessed by crystal violet staining, and growth inhibition (GI %) was calculated as:

$$GI\% = \frac{OD_{control} - OD_{treated}}{OD_{control}} \times 100$$

All experiments were performed in triplicate.

Clinical sample collection and bacterial identification

From November 2025 to April 2026, urine samples were collected from catheterised patients at Al-Karama Hospital, Baghdad. Samples were cultured on MacConkey agar at 37 °C for 24 h. *K. pneumoniae* isolates were identified by colony morphology, Gram staining, biochemical tests, and the Vitek-2 system (BioMérieux, France). Antimicrobial susceptibility was determined by Vitek-2, and isolates resistant to ≥3 antibiotic classes were defined as multidrug-resistant (MDR). A subset of five highly resistant isolates (designated isolates 1–5) was selected for further synergy testing.

Biofilm formation assay

Biofilm formation was quantified using the crystal violet microtiter plate method as described by Stepanović et al. (11). Briefly, each isolate was cultured in brain heart infusion (BHI) broth overnight, adjusted to 0.5 McFarland standard, and 20 µL was added to 180 µL of BHI with 1 % glucose in 96-well plates. After 24 h static incubation at 37 °C, wells were washed, fixed with methanol, stained with 0.1 % crystal violet, and destained with ethanol-acetic acid. Optical density (OD) was read at 630 nm. The cut-off (ODc) was defined as the mean OD of negative controls plus three standard deviations. Isolates were classified as non-biofilm producers (OD ≤ ODc), weak (ODc < OD ≤ 2×ODc), moderate (2×ODc < OD ≤ 4×ODc), or strong (OD > 4×ODc). The five isolates with the highest OD values (strong biofilm formers) were selected for synergy testing.

Antibacterial and synergy testing

The five selected isolates were exposed to:
Ag@Se nanoparticles at 25, 50, and 75 µg/mL
Meropenem at 2 and 4 µg/mL
Combinations of Ag@Se and meropenem (all nine combinations)
Negative control (no treatment)
Each condition was tested in triplicate. Growth inhibition was measured after 24 h by OD at 600 nm. The fractional inhibitory concentration (FIC) index was calculated as:

$$FIC = \frac{C^{comb}_{Ag@Se}}{MIC_{Ag@Se}} + \frac{C^{comb}_{MEM}}{MIC_{MEM}}$$

Synergy was defined as FIC ≤ 0.5, additivity as 0.5 < FIC ≤ 1, indifference as 1 < FIC ≤ 4, and antagonism as FIC > 4. Isobolograms were constructed, and combination indices were calculated using CalcuSyn software.

Statistical analysis

Data were expressed as mean ± standard deviation (SD) from three independent experiments. Comparisons between groups were performed using two-way analysis of variance (ANOVA) followed by Tukey's post-hoc test for multiple comparisons. A *P*-value < 0.05 was considered statistically significant. GraphPad Prism version 8.4 (GraphPad Software, USA) was used for all analyses.

Results

Physicochemical characterisation of nanoparticles

The UV-Vis spectrum of Ag nanoparticles showed a broad surface plasmon resonance (SPR) peak between 400 and 430 nm, indicating successful reduction of Ag^+ ions (Figure 1A). The peak broadening suggested a wide particle size distribution and some aggregation, consistent with plasma synthesis without stabilisers. For Ag@Se nanoparticles, the SPR peak exhibited a significant redshift (to longer wavelengths) and further broadening (Figure 1B), reflecting changes in the local dielectric environment due to selenium shell deposition.

XRD analysis of Ag nanoparticles revealed diffraction peaks at 2θ values corresponding to the (111), (200), (220), and (311) planes of a face-centred cubic (FCC) silver structure (JCPDS No. 04-0783). The dominant (111) peak indicated preferential orientation (Figure 2A). For Ag@Se nanoparticles (Figure 2B), the silver peaks remained prominent, confirming that the crystalline core was preserved after selenium deposition. Selenium-related peaks were weak and broad, suggesting an amorphous or poorly crystalline shell.

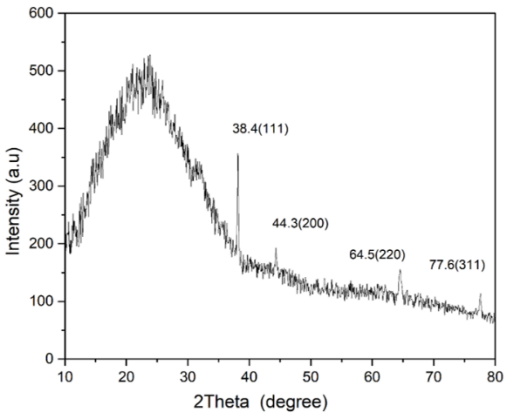


Figure 2A: XRD pattern of plasma-synthesized Ag nanoparticles, verifying a face-centered cubic (FCC) crystalline structure

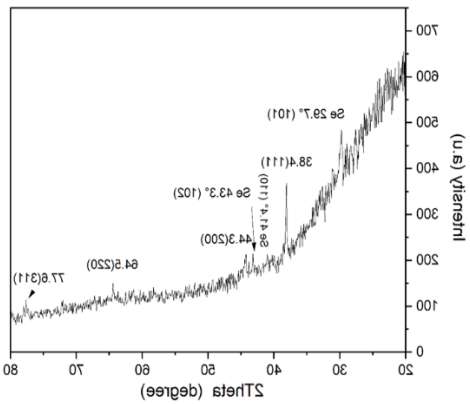


Figure 2B: XRD pattern of Ag@Se nanostructures, indicating that the Ag core crystalline structure remains intact following Se deposition

TEM micrographs (Figure 3) confirmed the formation of core–shell structures with an average diameter of approximately 100 nm. The silver core appeared as a dark, electron-dense region, while the selenium shell was lighter and somewhat irregular, indicating an island-type (Volmer–Weber) growth mode. Network-like aggregation was also observed, typical of diffusion-limited aggregation during plasma synthesis.

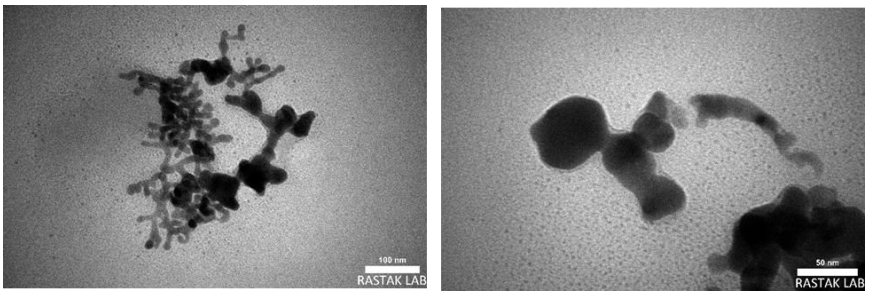


Figure 3: TEM micrograph of Ag@Se nanostructures, validating the core–shell formation with the dark Ag core and lighter Se shell

Cytotoxicity on normal REF cells

Ag@Se nanoparticles showed concentration- and time-dependent growth inhibition of REF cells (Table 1, Figure 4). At the highest tested concentration (100 µg/mL), growth inhibition was 17.7 % after 24 h and 23.3 % after 48 h. Even at 48 h, inhibition remained below 25 %, indicating relatively low cytotoxicity. There was no concentration at which inhibition exceeded 25 %, suggesting an acceptable safety profile for this normal cell line.

Table 1: Cytotoxicity of Ag@Se nanoparticles on REF cells (mean ± SD, n=3)

Concentration (µg/mL)	Growth inhibition (%) – 24 h	Growth inhibition (%) – 48 h
12.5	6.7 ± 1.5	9.0 ± 2.0
25	10.0 ± 1.0	15.0 ± 1.0
50	13.3 ± 2.5	17.7 ± 2.1
100	17.7 ± 1.5	23.3 ± 4.2

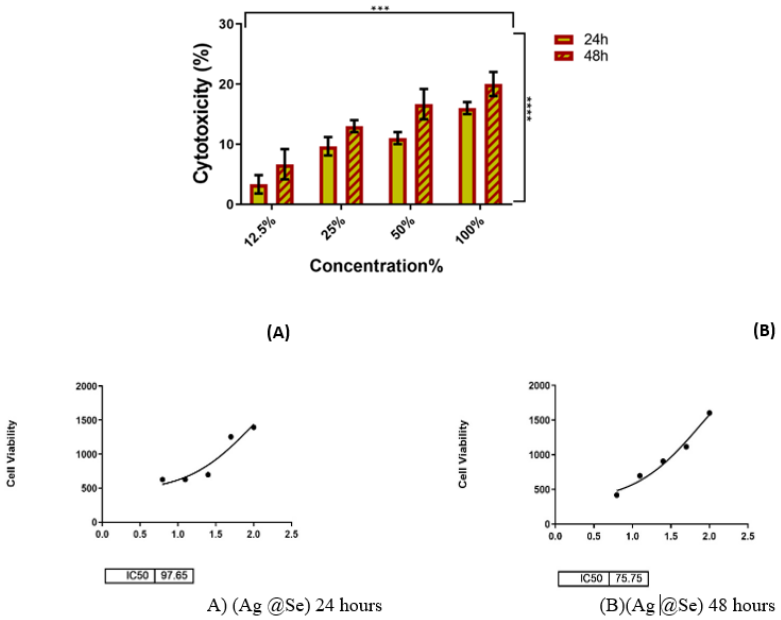


Figure 4: The cytotoxicity of Ag@Se nanoparticles after 24h and 48h on the REF cell line

Bacterial isolation and biofilm formation

Of 200 urine samples, 67 (33.5 %) were identified as *K. pneumoniae*. Among these, 30 isolates (44.8 %) were MDR. Biofilm formation was assessed for all 30 MDR isolates. The cut-off ODc was calculated as 0.105, based on negative control wells (mean = 0.054, SD = 0.017). Using the classification criteria, five isolates (IDs 1–5) showed strong biofilm formation (OD > 4×ODc = 0.420), with OD values of 0.639, 0.576, 0.569, 0.555, and 0.474, respectively (Table 2). These five isolates were selected for further synergy testing.

Table 2: Biofilm formation (OD_{630}) of 30 MDR *K. pneumoniae* isolates (top ten shown)

Isolate ID	OD_{630}	Biofilm classification
1	0.639	Strong
2	0.576	Strong
3	0.569	Strong
4	0.555	Strong
5	0.474	Strong
6	0.461	Moderate
7	0.46	Moderate
8	0.449	Moderate
9	0.448	Moderate
10	0.445	Moderate
...	...	...
30	0.236	Moderate

Antibacterial activity of Ag@Se nanoparticles alone

Against the five strong biofilm-forming isolates, Ag@Se nanoparticles exhibited concentration-dependent growth inhibition (Table 3). The highest inhibition for each isolate at the maximum tested concentration (75 µg/mL) was: isolate 1 – 62 %, isolate 2 – 58 %, isolate 3 – 61 %, isolate 4 – 65 %, and isolate 5 – 50 %. Moderate inhibition (40–55 %) was observed at 50 µg/mL, while 25 µg/mL yielded lower effects (20–35 %).

Table 3: Growth inhibition (%) of Ag@Se nanoparticles alone against five *K. pneumoniae* isolates

Isolate	25 µg/mL	50 µg/mL	75 µg/mL
1	28	48	62
2	22	52	58
3	35	61	61
4	30	65	58

5 20 35 50

Synergistic effect of Ag@Se nanoparticles with meropenem

Combining Ag@Se nanoparticles with meropenem substantially increased growth inhibition compared to either agent alone (Table 4). The highest inhibition for each isolate was observed with 75 µg/mL Ag@Se + 4 µg/mL meropenem for isolates 1, 2, 3, and 4 (70 %, 68 %, 70 %, and 68 %, respectively), and 50 µg/mL Ag@Se + 4 µg/mL meropenem for isolate 5 (60 %). The FIC indices ranged from 0.38 to 0.48, indicating true synergy (FIC ≤ 0.5) for all five isolates.

Table 4: Maximum growth inhibition (%) for combination treatments and FIC indices

Isolate	Best combination (Ag@Se / meropenem)	Inhibition (%)	FIC index	Interpretation
1	75 µg/mL / 4 µg/mL	70	0.42	Synergy
2	75 µg/mL / 4 µg/mL	68	0.48	Synergy
3	50 µg/mL / 4 µg/mL	70	0.38	Synergy
4	50 µg/mL / 4 µg/mL	68	0.44	Synergy
5	50 µg/mL / 4 µg/mL	60	0.46	Synergy

Discussion

This study successfully synthesised Ag@Se core–shell nanoparticles using a green cold plasma method and demonstrated their synergistic antibacterial and antibiofilm activity with meropenem against MDR *K. pneumoniae*. The findings address a critical need for new strategies to combat catheter-associated UTIs, where biofilms and multidrug resistance severely limit treatment options.

Characterisation and synthesis advantages

The plasma-assisted synthesis produced stable Ag@Se nanoparticles without toxic reducing agents, consistent with previous reports (9, 10). The redshift in SPR peak upon selenium addition confirmed successful shell formation, while XRD indicated retention of the crystalline silver core. TEM revealed core–shell morphology with partial, irregular selenium coverage – a feature of the Volmer–Weber growth mode often observed in plasma-mediated synthesis due to rapid nucleation and limited diffusion (12). Although full characterisation (e.g., EDS, XPS) would further confirm elemental distribution, the combination of UV-Vis, XRD, and TEM provides strong evidence for core–shell architecture.

Cytotoxicity profile

Ag@Se nanoparticles exhibited low toxicity against REF cells, with maximum growth inhibition of only 23.3 % after 48 h at 100 µg/mL. This is comparable to or better than many chemically synthesised silver nanoparticles, which often show significant cytotoxicity at similar concentrations (13). The relatively benign profile may be attributed to the selenium shell, which can modulate silver ion release and reduce direct cell membrane damage (14). Nevertheless, the study is limited to one normal cell line; further testing on human cell lines and in vivo models would strengthen safety claims.

Biofilm formation in clinical isolates

Among the 30 MDR isolates, nearly 17 % (5/30) were strong biofilm producers, a proportion similar to other reports from hospital settings (15). The strong biofilm formers (OD > 0.420) were preferentially selected for synergy testing because biofilms are a major therapeutic hurdle. The microtiter plate method used here is widely accepted, though it measures total biomass rather than viable cells within biofilms (11).

Synergistic antibacterial activity

The combination of Ag@Se nanoparticles with meropenem consistently outperformed either agent alone across all five isolates. The synergy (FIC indices 0.38–0.48) likely arises from complementary mechanisms: silver nanoparticles disrupt bacterial cell membranes and generate ROS, while meropenem inhibits cell wall synthesis; the disrupted membrane may facilitate greater antibiotic penetration (16, 17). Additionally, selenium nanoparticles themselves have been reported to downregulate biofilm-associated genes and impair matrix production (18). This triple action – membrane disruption, ROS production, and antibiofilm effect – may explain the enhanced activity against MDR *K. pneumoniae*, which often overproduces efflux pumps and carbapenemases.

Interestingly, isolate 5 showed lower overall susceptibility (max 60 % with combination) despite also being a strong biofilm former. This suggests strain-specific differences in resistance mechanisms, perhaps including carbapenemase production or altered porin expression, which future molecular studies could elucidate.

Comparison with previous studies

To our knowledge, this is the first report of Ag@Se core–shell nanoparticles combined with meropenem against *K. pneumoniae*. Prior work

by Hasan and Al-Awady (8) showed that berberine-loaded selenium nanoparticles inhibited *K. pneumoniae* and *Candida albicans*, but without antibiotic synergy. Another study using plasma-synthesised gold and silver nanoparticles demonstrated caspase-independent apoptosis in cancer cells (10, 19), highlighting the versatility of plasma methods. Our synergy findings extend the potential of plasma-synthesised nanoparticles to infectious diseases, particularly those involving biofilms.

Study limitations and future directions

Several limitations should be acknowledged. First, we did not measure the minimum inhibitory concentration (MIC) of meropenem alone for each isolate, relying instead on fixed sub-MIC concentrations (2 and 4 µg/mL). However, the consistent synergy across isolates suggests the effect is robust. Second, the study is entirely in vitro; in vivo validation using animal models of catheter-associated UTI is needed before clinical translation. Third, the mechanism of synergy was not directly investigated (e.g., ROS quantification, gene expression of efflux pumps or biofilm regulators). Future work should include transcriptomic analysis to identify pathways affected by the combination. Fourth, long-term stability and shelf-life of the plasma-synthesised nanoparticles were not assessed. Finally, while REF cells are a standard normal cell model, additional human cell lines (e.g., kidney epithelial cells) would provide a more comprehensive safety profile.

Future directions should focus on optimising the core–shell ratio for maximal synergy, testing the combination against a larger panel of carbapenem-resistant *K. pneumoniae* strains, and developing a catheter-coating formulation that releases Ag@Se and meropenem locally to prevent biofilm formation.

Conclusion

This study demonstrates that cold atmospheric plasma synthesis is an effective, eco-friendly method for producing Ag@Se core–shell nanoparticles with an average size of 100 nm. These nanoparticles exhibited low cytotoxicity against normal REF cells and showed significant antibacterial activity against MDR, biofilm-forming *Klebsiella pneumoniae* isolated from catheter-related UTIs. When combined with meropenem, Ag@Se nanoparticles produced synergistic growth inhibition (up to 70 %) with FIC indices indicating true synergy. The findings support the potential of Ag@Se nanoparticles as an adjunctive therapy to enhance the efficacy of existing carbapenems against biofilm-associated, drug-resistant infections. Further in vivo studies are warranted to translate these promising in vitro results into clinical applications.

List of Abbreviations

Ag@Se: Silver selenium core–shell nanoparticle
AgNPs: Silver nanoparticles
ANOVA: Analysis of variance
BHI: Brain heart infusion
CAP: Cold atmospheric plasma
CFU: Colony-forming unit
CI: Combination index
DC: Direct current
EDS: Energy dispersive X-ray spectroscopy
ESBL: Extended-spectrum β-lactamase
FCC: Face-centred cubic
FBS: Foetal bovine serum
FIC: Fractional inhibitory concentration
GI: Growth inhibition
MDR: Multidrug-resistant
MEM: Meropenem
OD: Optical density
ODc: Cut off optical density
REF: Rat embryo fibroblast
ROS: Reactive oxygen species
RPMI: Roswell Park Memorial Institute medium
SD: Standard deviation
SeNPs: Selenium nanoparticles
SPR: Surface plasmon resonance
TEM: Transmission electron microscopy
UTI: Urinary tract infection
XRD: X-ray diffraction

Declarations

Ethics Approval and Consent to Participate

The study was approved by the Institutional Ethics Committee of Al-Iraqia University, College of Medicine (approval number: IRB-COM-2025-034). All patient samples were collected after obtaining written informed consent from participants or their legal guardians. The study complied with the Declaration of Helsinki.

Consent for Publication

All authors gave consent for the publication of this work under the Creative Commons Attribution Non-Commercial 4.0 license.

Data Availability

The datasets generated and analysed during the current study are available from the corresponding author on reasonable request.

Competing Interests

The authors declare no competing interests.

Funding

This research received no specific grant from any funding agency in the public, commercial, or not-for-profit sectors.

Author Contributions

YEF worked on the conceptualisation, investigation, methodology, formal analysis and writing the original draft.
JSK worked on the methodology, validation, resources, writing the review and editing.
MMS worked on the conceptualisation, supervision, project administration, data curation, corresponding author, writing the review and editing.

Acknowledgements

The authors thank the staff of Al-Karama Hospital, Baghdad, for assistance with sample collection, and the Biotechnology Centre at Al-Nahrain University for providing cell culture facilities.

References

1. Shah AA, Alwashmi AS, Abalkhail A, Alkahtani AM. Emerging challenges in Klebsiella pneumoniae: Antimicrobial resistance and novel approach. Microbial Pathogenesis. 2025 May 1;202:107399. https://doi.org/10.1016/j.micpath.2025.107399
2. Haidar A, Muazzam A, Nadeem A, Atique R, Saeed HA, Naveed A, Sharif J, Perveen A, Fatima HR, Samad A. Biofilm formation and antibiotic resistance in Pseudomonas aeruginosa. The Microbe. 2024 Jun 1;3:100078. https://doi.org/10.1016/j.microb.2024.100078
3. Jalil MB, Al Atbee MY. The prevalence of multiple drug resistance Escherichia coli and Klebsiella pneumoniae isolated from patients with urinary tract infections. Journal of Clinical Laboratory Analysis. 2022 Sep;36(9):e24619. https://doi.org/10.1002/jcla.24619
4. Hetta HF, Alanazi FE, Ali MA, Alatawi AD, Aljohani HM, Ahmed R, Alansari NA, Alkhathami FM, Albogmi A, Alharbi BM, Alanzi HS. Hypervirulent Klebsiella pneumoniae: Insights into virulence, antibiotic resistance, and fight strategies against a superbug. Pharmaceuticals. 2025 May 15;18(5):724. https://doi.org/10.3390/ph18050724
5. Tian T, Han H, Guan ZH, Zhang K, Huang X, Wang W, Zhang X, Zhang F, Wei L, Zhang X, Wang JH. A systematic review of hypervirulent Klebsiella pneumoniae research: bibliometric and topic modeling perspectives. Frontiers in Medicine. 2025 Apr 11;12:1545678. https://doi.org/10.3389/fmed.2025.1545678
6. Shon AS, Bajwa RP, Russo TA. Hypervirulent (hypermucoviscous) Klebsiella pneumoniae: a new and dangerous breed. Virulence. 2013 Feb 15;4(2):107-18. https://doi.org/10.4161/viru.22718
7. Elbehiry A, Abalkhail A. Antimicrobial nanoparticles against superbugs: mechanistic insights, biomedical applications, and translational frontiers. Pharmaceuticals. 2025 Aug 13;18(8):1195. https://doi.org/10.3390/ph18081195
8. Hasan MF, Al-Awady MJ. The impact of berberine loaded selenium nanoparticles on K. pneumoniae and Candida albicans antibiotics resistance isolates. Archives of Razi Institute. 2023 Jun 30;78(3):1005. https://doi.org/10.22092/ARI.2022.359898.2509
9. Natsuki J, Natsuki T, Hashimoto Y. A review of silver nanoparticles: synthesis methods, properties and applications. Int. J. Mater. Sci. Appl. 2015 Sep 29;4(5):325-32. https://doi.org/10.11648/j.ijmsa.20150405.17
10. Mohammed MS, Adil BH, Obaid AS, Al-Shammari AM. Plasma jet prepared gold and silver nanoparticles to induce caspase-independent apoptosis in digestive system cancers. InMaterials Science Forum. Trans Tech Publications Ltd. 2022 Feb 18:1050;51-63. https://doi.org/10.4028/www.scientific.net/MSF.1050.51
11. Stepanović S, Vuković D, Hola V, Bonaventura GD, Djukić S, Ćirković I, Ruzicka F. Quantification of biofilm in microtiter plates: overview of testing conditions and practical recommendations for assessment of biofilm production by staphylococci. Apmis. 2007 Aug;115(8):891-9. https://doi.org/10.1111/j.1600-0463.2007.apm_630.x
12. Nominé AV, Gries T, Noel C, Nominé A, Milichko V, Belmonte T. Synthesis of nanomaterials by electrode erosion using discharges in liquids. Journal of Applied Physics. 2021 Oct 21;130(15). https://doi.org/10.1063/5.0040587
13. Rai M, Yadav A, Gade A. Silver nanoparticles as a new generation of antimicrobials. Biotechnology Advances. 2009 Jan 1;27(1):76-83. https://doi.org/10.1016/j.biotechadv.2008.09.002
14. Huang X, Chen X, Chen Q, Yu Q, Sun D, Liu J. Investigation of functional selenium nanoparticles as potent antimicrobial agents against superbugs. Acta Biomaterialia. 2016 Jan 15;30:397-407. https://doi.org/10.1016/j.actbio.2015.10.041

15. Ofem O, Deji-Agboola AM, Akinleye WA, Orizu CB. Molecular detection of ESBL genes in urinary pathogens from hospitalised and community patients in Ogun State, Nigeria. Babcock University Medical Journal. 2025 Dec 31;8(2):95-104. https://doi.org/10.38029/babcockuniv.med.j..v8i2.736
16. Burmistrov DE, Shumeyko SA, Semenova NA, Dorokhov AS, Gudkov SV. Selenium nanoparticles (Se NPs) as agents for agriculture crops with multiple activity: A review. Agronomy. 2025 Jun 29;15(7):1591. https://doi.org/10.3390/agronomy15071591
17. Yapa PN, Munaweera I, Weerasekera MM, Weerasinghe L. Nanoarchitectonics for synergistic activity of multimetallic nanohybrids as a possible approach for antimicrobial resistance (AMR). JBIC Journal of Biological Inorganic Chemistry. 2024 Aug;29(5):477-98. https://doi.org/10.1007/s00775-024-02066-w
18. Wadhwani SA, Shedbalkar UU, Singh R, Chopade BA. Biogenic selenium nanoparticles: current status and future prospects. Applied Microbiology and Biotechnology. 2016 Mar;100(6):2555-66. https://doi.org/10.1007/s00253-016-7300-7
19. Mohammed MS, Altaee MF, Al-Shammari AM. Retinoic Acid Treatment of Human Hematological Malignancies Induces Caspase Dependent and Independent Apoptotic Cell Death. Indian Journal of Forensic Medicine & Toxicology. 2021 Jan 1;15(1):1323. https://doi.org/10.37506/ijfmt.v15i1.13598